Sādhanā (2020)45:167
https://doi.org/10.1007/s12046-020-01408-z

Investigations on microstructural and microhardness developments in sintered iron–coal fly ash composites

AMARJIT SINGH[1], JARNAIL SINGH[1], MANOJ KUMAR SINHA[2], RAVI KUMAR[1] and VIKRAM VERMA[1,*]

[1]Department of Material Science and Engineering, National Institute of Technology, Hamirpur 177005, India
[2]Department of Mechanical Engineering, National Institute of Technology, Hamirpur 177005, India
e-mail: vermavikram11@gmail.com

MS received 31 January 2020; revised 24 May 2020; accepted 28 May 2020

Abstract. The present work is aimed to explore the microstructural and mechanical characteristics of coal-fly ash reinforced iron metal-matrix composites (IMMCs), synthesized through powder metallurgy technique. Coal-fly ash wt%, compacting load and sintering temperature were considered as the input variables, whereas sintered density and microhardness of the composites were taken as the output responses. Flowability and compressibility of the starting materials were demonstrated using Hausner ratio and Carr's index. Decorous morphological, crystallographic and elemental characteristics of the starting materials and IMMCs were deliberated using Scanning electron microscopy, X-ray diffraction and Energy-dispersiveX-ray spectroscopy investigations respectively. A significant improvement in the microhardness of IMMCs by 50% and drop in density by 35% were found at 15 wt% as compared to 0 wt% reinforcement. The substantial increase in the microhardness eventually resulted in an increase in their specific microhardness by a factor of two. Significant improvements in the microhardness of IMMCs at 15 wt % of reinforcement, compacted at 10 ton and sintered at 1150°C were found to be prompted by the strengthening mechanisms like load transfer, Hall–Petch effect and Taylor strengthening. The analytically calculated microhardness in the light of strengthening mechanisms was found smaller than the corresponding experimental values as a function of wt % of reinforcement. Further, statistical analysis of the obtained results was carried out using response surface methodology.

Keywords. Metal-matrix composites; coal-fly ash; powder metallurgy; microhardness; strengthening mechanisms; sintered density.

1. Introduction

Coal-fly ash reinforcements are being used abundantly in fabricating various engineering materials like bricks, cement and metal-matrix composites (MMCs). Specifically, low weight MMCs are being fabricated by reinforcing inexpensive coal-fly ash successfully to enhance their mechanical and tribological properties [1]. Such materials are being used extensively in aerospace, automobile, aviation, marine, sports and power industries. Coal-fly ash mostly contains spherical particles of SiO_2, Al_2O_3, Fe_2O_3 and TiO_2 with varying particle size ranges from 1 μm to 100 μm. The coal-fly ash is a mixture of dense and hollow particles which are generally termed as precipitator and cenosphere, respectively [2–4]. Precipitator particle reinforcement is commonly used for inducing favourable mechanical properties such as hardness, stiffness, wear resistance, etc. in relatively soft metal matrices. As per ASTM C618, Indian coal-fly ash falls in the F-category which contains at least 70 % SiO_2 and Al_2O_3. Contribution of SiO_2 particles in F coal-fly ash is more than 50%, hence used to strengthen the MMCs through excellent load-bearing mechanisms [5–7].

The resultant properties of MMCs primarily depend on the type, amount and distribution of the reinforcement into the matrix. Owing to the poor wettability and low density of ceramic reinforcements as compared to the matrices, liquid state fabrication method of MMC results in their non-uniform distribution in the matrix. To overcome these problems, the powder metallurgy (PM) technique is broadly used as a solid-state method to fabricate denser, precise, high strength MMCs. The upper limits of the reinforcements which can be accommodated into the metal-matrix using PM and stir casting process are 50% and 30%, respectively [8–11]. This signifies that using PM uniform dispersion and a higher amount of the reinforcements leads to a wider scope of tailoring the properties of MMCs.

*For correspondence
Published online: 27 June 2020

Recently, Sahoo *et al* [12] synthesized MMCs through PM technique to study the effects of TiB_2 reinforcement on stainless steel (AISI 304) matrix. The effect of vol. % of reinforcement and sintering parameters on densification, hardness and deformation of the MMCs were evaluated using microhardness and nanoindentation techniques. A significant enhancement in hardness, elastic modulus and strength of the MMCs was explained based on uniform distribution of 4 vol. % of reinforcement at sintering temperature of 1100°C. Abdollahi *et al* [13] optimized PM parameters being used to fabricate parts from Iron and grey cast iron powders. Effects of cast iron powder percentage, compaction pressure, sintering temperature and time were investigated on the density, transverse rupture strength and hardness of the sintered samples. It was concluded that iron jet-milled grey cast iron powder is more economical for producing PM parts with diverse properties. Zhang *et al* [14] presented the effect of the amount of graphite and sintering temperature on microstructural and mechanical properties of iron. It has been found that the increased amount of graphite from 5 to 20% and sintering temperature from 600°C to 1100°C resulted in significant improvement of mechanical properties. The hardness enhancement took place due to the lattice distortion resulted by the formation of Fe_3C at an increased amount of graphite and high sintering temperatures. Sharma *et al* [15] characterized the iron-alumina MMCs for structural and mechanical behaviour studies. Iron with 5wt % alumina powders were ball milled and compacted at 10, 12.5 and 15 KN loads and annealed at 900, 1000 and 1100°C for one hour respectively. Density and hardness of fabricated specimens were evaluated and discussed based on the well-dispersed dense nano iron-aluminate evolved in the microstructure of the MMCs. A significant enhancement in density from 4.7 to 5.51 g/cm^3 and hardness from 63 to 94 HRH has been witnessed. Gupta *et al* [16] investigated the sintering and hardness behaviour of Fe-Al_2O_3 nano-composite synthesized by PM route. Sintering of the green compacts was carried out in inert atmosphere at temperatures 900 to 1100°C for 1 to 3 hours. Dense nanophase of iron-aluminate formed due to reactive sintering between the powders was detected using Scanning electron microscopy (SEM) and X-ray diffraction (XRD). Sahoo *et al* [17] presented the mechanical properties and wear behaviour of MMC fabricated by the hot-pressed method using stainless steel as a matrix and TiB_2 as reinforcement. The contributions of different strengthening mechanisms in improving the properties of MMCs were quantified. Guo and Rohatgi [18] characterized the aluminium-coal-fly ash powder compacting process. Both precipitator and cenosphere particles were reinforced in the range of 5–20 wt. % to aluminium powder. Compaction was carried out in the range of 138 to 414 MPa. Green strength, green hardness, green density, spring back and densification parameters were studied as a function of compacting load and coal-fly ash wt.%. It has been reported that on increasing compacting load the green strength, green density and spring back exhibited increasing trends. Whereas the increased wt. % of coal-fly ash resulted in the reduction of green strength, green density, spring back and hardness of the compacted samples. Rajan *et al* [19] carried out the microstructural, electrical, thermal and tribological study of copper-coal-fly ash composites prepared by PM technique. The increased hardness and wear resistance has been found in the Cu-coal-fly ash composite as compared to the copper matrix. The optimum amount of coal-fly ash was found as 9 % as far as improvement in hardness and uniform distribution of reinforcement in the matrix is concerned. Beyond this amount of reinforcement, a decrease in electrical and thermal conductivity of the composite was reported. However, the coefficient of friction was not affected on enhanced coal-fly ash reinforcement, but the decrease in specific wear rates of the composite was found.

From the cited literature, it is evident that different metal matrices such as aluminium, steels etc. were reinforced with Al_2O_3, SiC and coal-fly ash to fabricate the MMCs. However, an insignificant number of research papers were found wherein reinforcement of inexpensive coal-fly ash to the pure iron matrix was used to fabricate MMCs. Therefore, the objective of the present work is to manifest the usefulness of inexpensive coal-fly ash as reinforcement to the iron matrix to enhance the mechanical properties of IMMCs fabricated thereof. The resultant properties of IMMC are discussed in the light of various strengthening mechanisms as a function of varying wt % of reinforcements. Further, statistical authentications of results of input variables are being carried out by RSM techniques using Design Expert 10 software.

2. Materials and methods

The commercially available atomized iron powder of purity 99.5% purchased from Sigma Aldrich Bangalore, India was used as matrix. Coal-fly ash introduced as reinforcement to the iron matrix was collected from Rajpura thermal power plant situated in Patiala district of Punjab, India. Design Expert 10 software was used for the Design of experiments (DoE). Bulk density and tap density of iron powder and coal-fly ash were calculated to exhibit their flowability and compressibility through Hausner ratio and Carr's index. Coal-fly ash was mixed with iron powder at different contents of 0, 7.5 and 15 wt% using a planetary ball milling machine. Tungsten carbide balls having diameter 10 mm (powder to ball ratio 1:10) was used as milling medium and machine was operated at 200 rpm for one hour. Subsequently, pallets were prepared from the mixed powders at different compacting pressure of 5, 7.5 and 10 tons; respectively. The prepared pallets were further sintered at temperatures of 950°C, 1050°C and 1150°C in a tubular furnace for one hour under inert environment. The sintered

densities of pallets were calculated as per ISO 3369:1975 using Archimedes method and using equation (2). X-ray diffraction (PANanalytical X'Pert PRO, MPD, Netherlands) having a wavelength (λ) 1.54 Å operated at 40 *m*A, 45 kV was performed for structural characterization of starting powders as well as sintered pallets. Data were recorded in the range of 20 to 80° with a step size of 0.02° and a scan speed of 2°/min. Field emission scanning electron microscopy (FESEM) (FEI Quanta FEG-450) was used to demonstrate the morphology of starting materials and pallets. Elemental analysis of the starting materials was carried out using Energy-dispersive X-ray spectroscopy (EDS). Microhardness of prepared composites was recorded using Vickers microhardness (Wilson instrument, Model 401/402 MVD, UK) operated at a load 50 g for a dwell time of 10 sec. To authenticate the effects of various input parameters on the responses: couture, surface and perturbation graphs were plotted using RSM. Analysis of variance and regression models were also derived for each response. The contribution of various strengthening mechanisms involved in improved microhardness of composites was exhibited. The density reduction and enhanced microhardness of the composite were discussed and analysed statistically in the light of microstructural evolution and various strengthening mechanisms.

3. Results and discussions

3.1 *Elemental and compositional analysis of the starting materials*

An EDS technique was used to identify the elemental composition of starting powder samples. EDS of iron powder has depicted 99.5% Fe content. On the contrary, coal-fly ash found to be composed of multi-components such as SiO_2, Al_2O_3, Fe_2O_3, TiO_2 and K_2O as shown in table 1. SiO_2, Al_2O_3 and Fe_2O_3 are key elements of the coal-fly ash which is completely in agreement with our XRD findings.

3.2 *Flowability and compressibility evaluation of the starting powders*

In the powder metallurgy techniques, the flowability of powder plays an important role in compacting the powder with minimal porosity at a given pressure and temperature. The bulk and tap densities of the powders largely depend on the size and shape of the particles and influence the flowability of the powders. Hausner ratio and Carr's index are often used to exhibit the flowability and the compressibility of powder-like materials [20]. Hausner ratio is the ratio of tap density to the bulk density and always remains ≥ 1. Its value ≥ 1.25 is the indication of poor flowability of the powder. Carr's index is also known as compressibility index and is expressed as given in table 2. The powders exhibiting Carr's index ≥ 25 is the indication of poor flowability and the values ≤ 15 is considered as good flowability. The iron powder and coal-fly ash were undertaken to manifest their suitability for powder metallurgy through calculating their Hausner ratio and Carr's index. These starting materials exhibited good flowability and compressibility as the numerical values of Hausner ratio and Carr's index well in ranges as depicted in table 2 [21].

Table 1. Constituents of the coal-fly ash.

Compound	SiO_2	Al_2O_3	Fe_2O_3	TiO_2	K_2O
Percentage (%)	58.34	33.88	3.03	2.12	2.12

3.3 *Morphology of the starting materials and the composites*

FESEM micrographs of as-received iron powder, coal-fly ash and sintered pallets of IMMCs with different amounts of coal-fly ash are depicted in figures 1(a-e). Figures 1 (a-b) illustrate the dense and spherical shaped iron and coal-fly ash particles. The particles size of as received coal-fly ash is not uniform and ranges from 75 μm to 100 μm. Generally, the spherical morphology is advantageous to synthesise MMCs as far as powder mixing, compaction and solid-state sintering are concerned. Figures 1(c-e) depicts the micrographs of the pallets reinforced with different amounts of coal-fly ash. Few black dots are also being observed in the micrograph, exhibiting the porosity of IMMCs. Whereas, the coal-fly ash reinforced IMMCs, exhibits varying amounts of white spots confirm the proper dispersion of coal-fly ash surrounded by dense iron matrix. As the coal-fly ash content increases, more and more white spots have been detected in FESEM micrographs. A key observation is that the increased amount of reinforcement resulted in reduced inter-particle distance of the coal-fly ash particulates. This will certainly contribute to the enhanced microhardness of the prepared IMMCs by hindering the movement of dislocations during deformation of the matrix [17, 22].

3.4 *Microstructural analysis of the starting materials and the composites*

Figures 2 (a) is exhibiting the XRD patterns of coal-fly ash and as-prepared pallets of IMMCs reinforced with 0, 7.5 and 15 wt % coal-fly ash. XRD spectra of coal-fly ash illustrate a multi-component system comprising distinct phases such as SiO_2, Al_2O_3, Fe_2O_3 and mullite [6]. Sintered pallet with 0 wt % coal-fly ash exhibits the cubic crystal

Table 2. Hausner ratio and Carr's index of the starting materials.

Material	Bulk density (P_B)	Tap density (P_T)	Hausner ratio = (P_T/P_B)	Carr's index = $100\left(1-\frac{P_B}{P_T}\right)$
Iron powder	3.35 g/cm^3	3.80 g/cm^3	1.13	12
Coal-fly ash	0.70 g/cm^3	0.77 g/cm^3	1.10	10

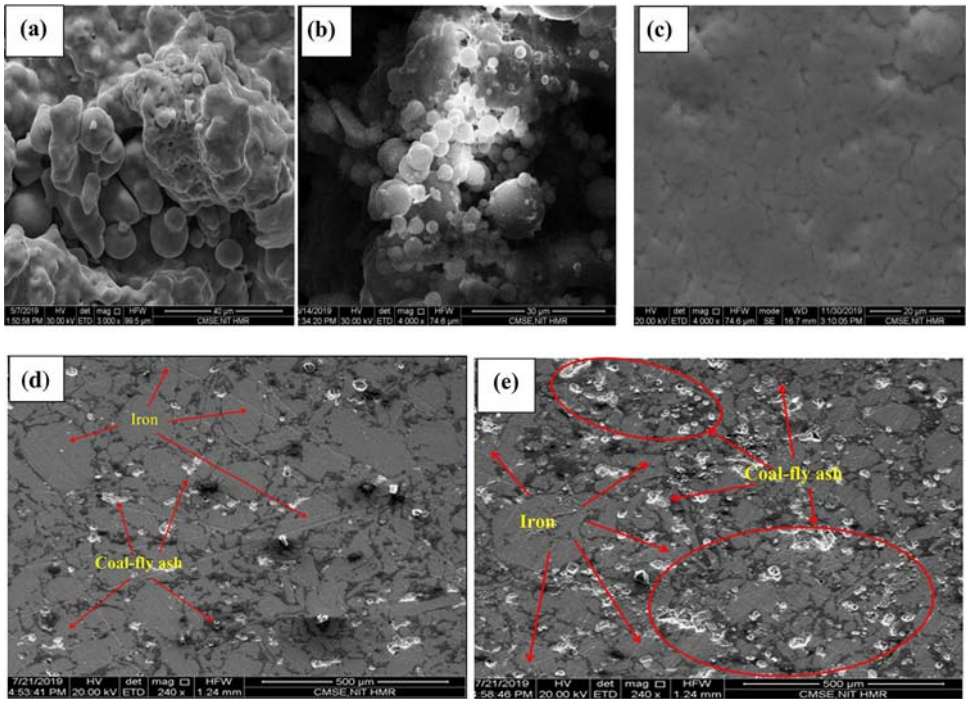

Figure 1. FESEM micrographs of: (**a**) iron powder, (**b**) coal-fly ash, (**c**) IMMC 0 wt% coal-fly ash, (**d**) IMMC 7.5 wt% coal-fly ash and (**e**) IMMC 15 wt% coal-fly ash.

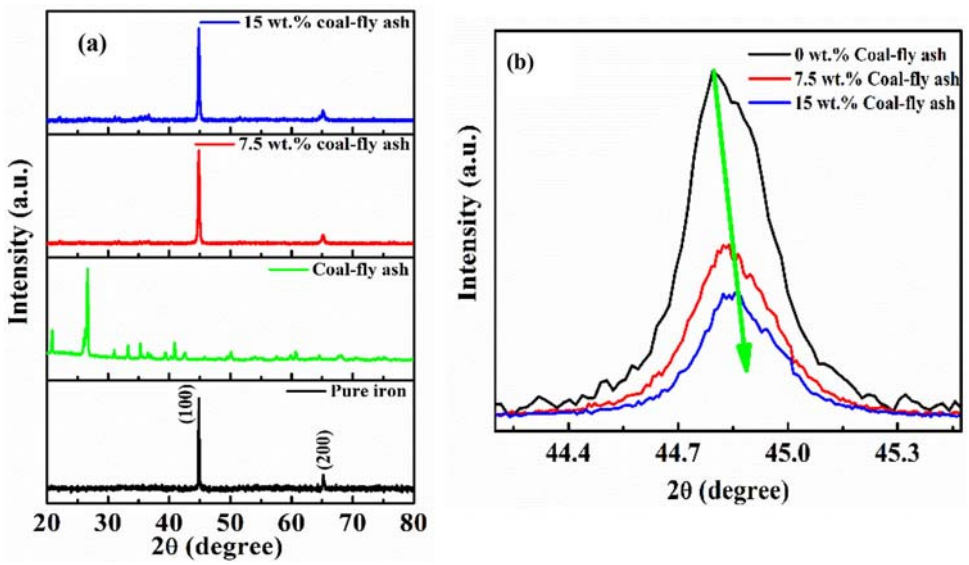

Figure 2. X-ray diffraction patterns: (**a**) 0 wt% coal-fly ash reinforced composite, coal-fly ash particulates, 7.5 wt% coal-fly ash reinforced composite, 15 wt% coal-fly ash reinforced composite and (**b**) shifting and broadening of peaks as a result of reinforcement.

structure, which is in agreement with JCPDS card number 89-7194. Two peaks reflected in the pattern at 44.67° and 65.02° correspond to (110) and (200) planes respectively alike to the pure iron and indicate that there is no formation of the secondary phase. However, peak corresponds to (110) plane found to be more intense which means that crystallographic direction of (110) plane increases with the sintering temperature.

The XRD spectra of the IMMCs with coal-fly ash contents of 7.5 and 15 wt % are also shown in figure 2 (a). In both sintered pallets combined spectra of pure iron powder and coal-fly ash have been observed without the formation of the third phase. However, all peaks corresponding to coal-fly ash are difficult to distinguish from backgrounds due to higher crystallinity of the iron phase. Shifting and broadening of peaks exhibited in figure 2 (b) is confirming the strain induced in the structure of the matrix resulting from the incorporation of coal-fly ash. The average grain size for all pallets was calculated by using Scherrer's equation as shown in equation (1) [23]:

$$D = \frac{0.9\lambda}{\beta \cos\theta} \tag{1}$$

where D, λ, β and θ are grain size, wavelength of incident X-rays, full width at half maximum (FWHM) and Bragg's angle; respectively. The average grain sizes of the matrix phase as a function of coal-fly ash wt% are summarized in table 3. Here, broadening and shifting of the peaks as a function of increased wt % of coal-fly ash might be contributing to the enhanced strength and microhardness of the composites.

3.5 *Evaluation of density of the composite*

The density of the as-sintered pallets was calculated using Archimedes principle. The weight of pallets was measured on a digital weighing machine both in air and in distilled water and densities were calculated as per equation (2)[24]:

$$\rho_c = \frac{\text{Weight of composite in air}}{\text{Weight of composite in air} - \text{Weight of composite in water}} \times 1 \tag{2}$$

where ρ_c is the density of composite and 1 is the density of water in g/cm^3. A marginal enhancement in the sintered densities of pallets was found, as a function of the compacting pressure and the sintering temperature. However, a significant drop in the sintered densities of pallets was witnessed as a function of increased coal-fly ash wt%. A quantitative effect of various input variables on responses is given in table 4. The evident reason for this drop in the density of composite is the huge difference in the densities of iron (7.87 g/cm^3) and coal-fly ash (2 g/cm^3) [10, 25]. The significant reduction in the density of the composite material is often prime requirement to establish the composite. A maximum 35 % reduction in the density has been found at 15 wt % of reinforcement.

Table 3. Varying grain sizes of the matrix as a function of wt % coal-fly ash.

Sl. no.	Coal-fly ash wt%	Grain size (nm)
1	0.0	55
2	7.5	36
3	15.0	33

3.6 *Evaluation of the microhardness*

Increased microhardness of the composite as a function of the input variables was measured using a Vickers microhardness (Wilson instrument, Model 401/402 MVD, UK) testing instrument. Before the measurement, the as-sintered composite pallets were polished as per standard procedures; subsequently,a load of 50 g was indented for 10 sec. Average of five such indentations on different parts of the pallets by the diamond pyramid was considered for calculating the microhardness value. It has been found that with the increased compacting pressure and sintering temperature, the microhardness of the pallets enhanced marginally. But, a significant enhancement in microhardness by 50 % was recorded at 15 wt % of reinforcement as compared to the 0 wt % of reinforcement as shown in table 4. Therefore, coal-fly ash wt % is found to be a dominating factor affecting the microhardness of IMMCs. In addition to the presence of hard ceramic particles like SiO_2 and Al_2O_3, various strengthening mechanisms might also be responsible for the increased pallets hardness.

3.7 *Strengthening mechanisms*

The enhancement in microhardness of MMCs cannot be understood completely based merely on the morphology, chemical compositions and mechanical properties of matrix and reinforcement materials. Particularly in the case of micrometric scaled particulate-reinforced MMCs, three strengthening mechanisms known as Load transfer strengthening (L_t), Hall–Petch effect (H_p) and Taylor's strengthening mechanism (T_y) predominate to be operative in the microstructure of the matrix [26]. These mechanisms significantly affect the microhardness of the composite through improvement in the yield strength (σ_y). These strengthening mechanisms and their contribution towards improved microhardness of IMMCs have been theoretically asserted, graphically represented and compared with experimental values in the subsequent sections [27].

Table 4. Input parameters and responses.

Sl. no.	Coal-fly ash wt% (g)	Compacting load (Ton)	Sintering temperature(°C)	Sintered density(g/cm^3)	Microhardness (Hv)
1	7.5	5	1150	5.48	137
2	7.5	10	950	5.77	132
3	7.5	7.5	1050	5.87	135
4	7.5	5	950	5.18	137
5	0	5	1050	6.85	110
6	7.5	7.5	1050	5.79	140
7	7.5	10	1150	5.84	166
8	0	7.5	950	6.96	116
9	0	7.5	1150	7.58	124
10	15	10	1050	5.11	161
11	15	5	1050	4.74	160
12	7.5	7.5	1050	5.83	142
13	15	7.5	1150	5.05	168
14	7.5	7.5	1050	5.71	149
15	7.5	7.5	1050	5.76	153
16	0	10	1050	7.36	134
17	15	7.5	950	4.71	145

3.7a *Load transfer strengthening (L_t):* On inclusion of the second hard phase to the soft matrix the bonding between reinforcement particulates and matrix improves the strength of a composite by activating the phenomenon of load transfer. Hence, the load transfer from the soft matrix phase is easily executed to harder reinforcement particles during plastic deformation of the material caused by the applied load during hardness measurements. The agglomeration free uniform distribution of coal-fly ash in the iron matrix is evident from figures 1 (d-e). This is exhibiting the favourable conditions of stronger and clear interfaces between the matrix phase and the reinforcement particulates [28]. In this work, the existence of more than 70% of hard and strong SiO_2 and Al_2O_3 particles in coal-fly ash are resulting in increased strength and hardness of the IMMCs. With the increased amounts of reinforcement, the microhardness of the IMMCs exhibiting significant improvements owing to the load transfer strengthening mechanism is presented as per the modified equation (3):

$$\Delta Hv_{Lt} \cong 2.8\Delta\sigma_{Lt} \cong 0.5V_p\sigma_m \tag{3}$$

where ΔHv_{Lt}, $\Delta\sigma_{Lt}$, $V_{p,}\sigma_m$ are an improvement of Vickers microhardness of composite, yield strength due to load transfer, the volume percentage of reinforcement and yield strength of matrix; respectively. It is a clear observation from figures 1 (d-e), that an enhanced amount of reinforcement eventually reduces their interparticle spacing. This is going to share more loads with the harder reinforcement particles as compared to the softer matrix. The graphical representation of the effect of load transfer mechanism is shown in figure 3 (a).Wherein, the load transfer mechanism is exhibiting a very steep effect with increased reinforcement from 0 wt % to 7.5 wt %. However, from 7.5 wt % to 15 wt % reinforcement the steepness got reduced [29].

3.7b *Hall–Petch effect (H_p):* Hall–Petch effect is another significant strengthening mechanism which is comprehensively accepted for the strengthening of metals, alloys and composites. As per this effect, during recrystallization, the inhibited grain growth in polycrystalline material cause the grain refinement and increased number of grain boundaries [30]. Thus, exponentially increased grain boundaries create more constraints for the dislocations motion during plastic deformation caused by the applied force of indentation. This renders higher stress generation and concentration in the material structure and the material behaves harder and stronger. The increase in hardness can be evaluated as per the relation shown in equation (4) [31]:

$$\Delta Hv_{Hp} \cong 2.8\Delta\sigma_{HP} \cong \frac{K_{HP}}{\sqrt{D}} \tag{4}$$

where ΔHv_{Hp}, $\Delta\sigma_{HP}$, K_{HP} and D are an increase in Vickers microhardness, change in yield strength, material constant and mean grain size; respectively. Coal-fly ash particulates reinforced to the iron matrix serves as nucleation sites during recrystallization. Thus, the increased amounts of reinforcement might be enhancing the number of grains in the matrix of IMMCs, which multiplies the grain boundaries and creating hurdles for free movement to the dislocations during plastic deformation resulted while indentation [32, 33].

The relation between grain refinement of the matrix phase extracted from the XRD data and the corresponding variations in microhardness of IMMCs as a function of reinforcement amounts is graphically shown in figure 3 (b). Wherein,a steep decrease in grain size and the

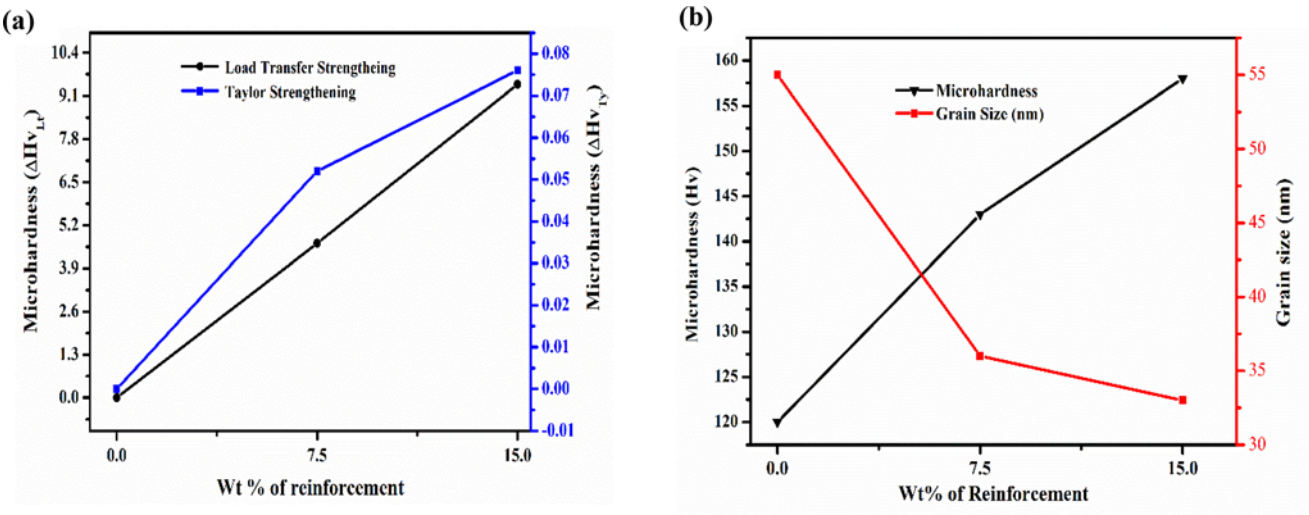

Figure 3. Effect of reinforcement amount: (**a**) microhardness as a function of Load transfer and Taylor strengthening and (**b**) on grain size and microhardness.

corresponding increase in microhardness is witnessed during the enhancement ofreinforcement from 0 to 7.5 wt %. Further, the intensity of reduction in grain size and enhancement in microhardness is reduced with reinforcements increased from 7.5 to 15 wt %. It can be inferred, that the Hall–Petch effect is playing a significant role in making the IMMCs stronger and harder through grain refinements [34].

3.7c *Taylor's strengthening mechanism (T_y):* To accommodate the significant difference in coefficient of thermal expansions (CTE) of reinforcement and matrix materials, geometrically necessary dislocations appear in the vicinity of reinforcement particles of the MMCs. Further, the dislocations density enhances as a function of increased amount and reduced size of the reinforcements [35]. In the present study, the coefficient of thermal expansion (CTE) of iron-matrix phase (12×10^{-6}/K) is almost double of coal-fly ash (6.1×10^{-6}/K). The above conditions are pointing towards Taylor's strengthening mechanism which might be active in the microstructure of composites. As per the established empirical relation between yield strength (σ_y) and microhardness of a material, the improvement in the microhardness (ΔHv_{Ty}) of the composite can be manifested vide the following modified equation (5)[36]:

$$\Delta Hv_{Ty} \cong 2.8\Delta\sigma_{Ty} \cong \beta Gmb\sqrt{\frac{12\Delta\alpha\Delta TVp}{bdp(1-Vp)}} \qquad (5)$$

where β, Gm and b are material specific constants i.e. strengthening coefficient, shear modulus and burgers vector of the matrix respectively. $\Delta\alpha$ and ΔT are differences in the coefficient of thermal expansion between matrix and reinforcement material and processing temperatures respectively. The terms dp and Vp represents the average particle size and volume % of reinforcement respectively. Hv is an enhancement in the Vickers microhardness of composite and $\Delta\sigma_{Ty}$ is the improvement in yield strength imparted by Taylor's strengthening. Hence, during sintering of IMMCs, this mismatch of CTE is generating geometrically necessary dislocations in the vicinity of reinforcement particles to release the thermal stresses [37–39]. The dislocation densities enhancement is taking place primarily due to the enhanced amounts reinforcement. Figure 3(a) indicates almost liner contribution of the reinforcement to the improvement of microhardness of IMMCs [26].

Increased reinforcement not only generates dislocations but also creates restrictions on the free movement of the dislocations as a result of reduced grain size of matrix and inter-particulate distance of the reinforcement [40]. Since the composites synthesised in this work exhibiting a significant increase in microhardness on increased reinforcement, hence it can be inferred that the above phenomenon might be active in the microstructure of the IMMCs [41]. A quantitative effect of various input variables on responses is given in table 4. Further, the contribution of each strengthening mechanisms (L_t, H_p and T_y) in improving the microhardness (ΔHv) of IMMCs are manifested by modified summation model as shown in equation (6) [42, 43]:

$$\Delta Hv \cong 2.8\left(\sigma_m + \Delta\sigma_{Ty} + \Delta\sigma_{Hp} + \Delta\sigma_{Lt}\right) \qquad (6)$$

To appraise the contribution of T_y, H_p and L_t in improving microhardness of the IMMCs, the computations were carried out using equations (3), (4), (5) and (6) and input variables as given in table 4. The results revealed that at 0 wt % of reinforcement only Hall Petch effect was active in improving the microhardness of the matrix (Hv_m). At 7.5 wt % of reinforcement, the increased H_p effect was followed by L_t and Taylor Strengthening. H_p followed by L_t and T_y mechanisms were found at maximum 15 wt % reinforcement, 10-ton compaction load and 1150°C

sintering temperature [26, 27]. Whereas, L_t found to be the dominating strengthening mechanism followed by H_p and T_y imparting significant improvements in microhardness of the IMMCs through improved yield strength. Further, the calculated values of microhardness were compared with the experimental (Hv_{Ex}) values. The experimental values were found significantly higher than the theoretical values except at 0 wt % of reinforcement. Synergistically strengthening mechanisms exhibiting increased microhardness of IMMCs as a function of wt % of reinforcement, which is well in line with the established research results. The possible reasons behind the changing trends of strengthening mechanisms are the constant particle size (75–100 μm) and varying wt % of the reinforcement [44]. The increased amount of reinforcement from 0 wt % to 7.5 wt % provided more number of nucleation sites in the matrix to grow more grains during sintering. As per table 3, the grain size of the matrix phase got refined from 55 nm to 36 nm and the presence of reinforcement particles also started sharing some load from matrix i.e., the Hp dominated L_t [29]. However, the difference between CTEs of reinforcement and matrix material is not sufficiently high and the amount of reinforcement is not sufficient i.e., T_y has a limited contribution. With further increase of reinforcement from 7.5 wt % to 15 wt % nucleation sites increased and grain size refined only from 36 nm to 33 nm. As per figures 1(d-e), the increased wt % of reinforcement significantly reduced the distance between its particles which enabled them to bear more load form the matrix i.e., L_t supersedes the H_p. Now the composite has sufficient amount of reinforcement which also enable the T_y got increased [42]. During the comparison, the experimental values of microhardness were found higher than that of theoretically calculated. The possible reason may be as follows: one due to other possible strengthening mechanisms active in microstructure the IMMCs, secondly generation and accumulation of inhomogeneous dislocation behind the micrometric sized particulates [45]. Contribution of each strengthening mechanism along with the comparison of calculated and experimental values of microhardness of the IMMCs as a function of wt % of reinforcement is shown graphically in figure 4.

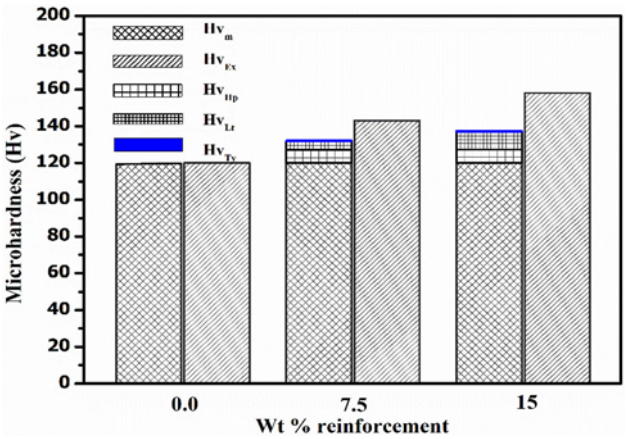

Figure 4. Comparison of theoretical and experimental microhardness and contribution of strengthening mechanisms in the IMMCs.

3.8 *Statistical analysis*

3.8a *Statistical analysis of the density:* In the statistical analysis of density, the F-value of the model has been found 112.35 which imply that the developed model is significant. The modified ANOVA table for the sintered density is presented in table 5. Among the input parameters A, B, C, AB, and AC, parameter A, i.e., coal-fly ash wt % found to be the most dominant factor affecting the sintered density. Lack of Fit F-value of 0.0617 implies that it is non-significant relative to the pure error which advocates the expected significance of the model. Statistical values of R^2 and R^2 (adj.) were found to be 0.99 and 0.98, respectively. The closeness of these values advocates the adequacy of the regression model developed. It also discards any possibility for further increase in the degree of the developed regression model. The developed model is sufficient enough to capture the variance in the observed experimental data. The regression model for the sintered density extracted from the analysis is given in equation (7):

$$\rho_c = 5.76 - 1.14 \times \mathrm{A} + 0.23 \times \mathrm{B} + 0.17 \times \mathrm{C} \quad (7)$$

The sintered density of the composites is significantly influenced by coal-fly ash wt. % in an inverse fashion. An overall reduction in composite density can also be attributed to the combined effect of porosity of the matrix and the lower density of the reinforcement [46]. The data obtained for sintered densities were also found uniformly distributed around the straight line as depicted in figure 5(a). The predicted and actual values of the sintered densities were found scattered randomly and do not follow a specific trend as shown by figure 5(b). The random distribution of the obtained data discards any possibilities of pre-biasing while experimentation. Increasing compact load is enhancing the sintering density through the increased green density. As the applied load during compaction of powders result in reduced porosity by reducing the interparticle distances of matrix and reinforcement as well. The experimental value of the sintered density of a sample with 0 wt % reinforcement achieved is 96.3 % of the theoretical density of matrix at maximum compacting load of 10 tons and 1150°C sintering temperature; respectively. Whereas, a minimum sintered density of 64.1 % of the theoretical density of pure iron is found at compacting load of 5 tons and 950°C sintering temperature at 15 wt % of the reinforcement.

Table 5. Modified ANOVA table for the sintered density.

Source of variation	Sum of squares	Degree of freedom	Mean square	F value	P-value
Regression	11.77	9	1.31	112.35	< 0.0001
A (Coal-fly ash wt%)	10.44	1	10.44	897.39	< 0.0001
B (Compacting load)	0.42	1	0.42	35.97	0.0005
C (Sintering temperature)	0.22	1	0.22	19.00	0.0033
Residual error	0.08	7	0.012		
Lack of Fit	0.066	3	0.022	5.77	0.0617
Pure Error	0.015	4	3.820E−003		
Total	11.85	16			

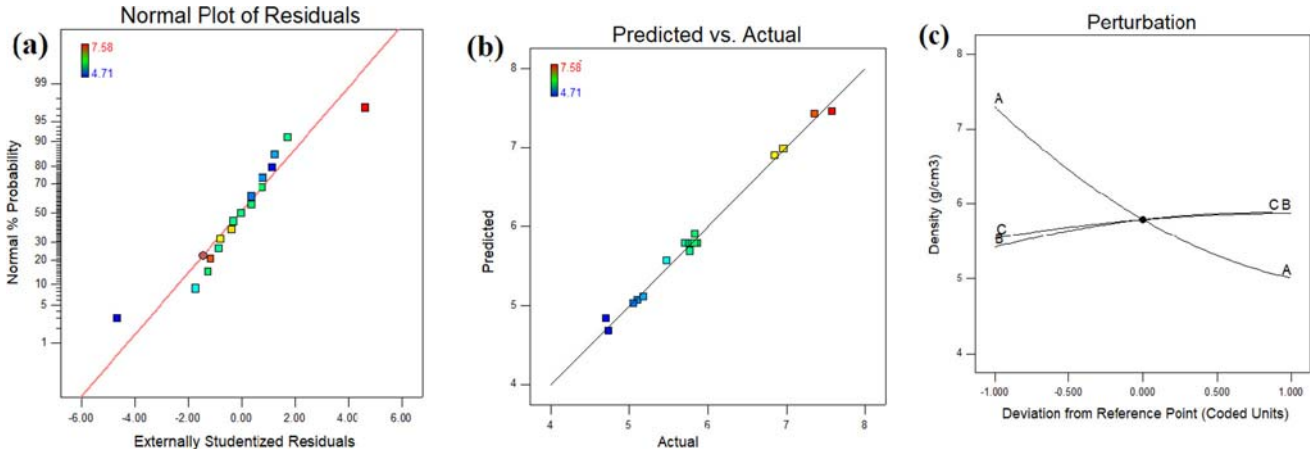

Figure 5. Plots for the sintered density: (**a**) normal probability plot, (**b**) predicted vs. actual and (**c**) perturbation plot.

The starting materials exhibited the expected compaction behaviours and resulted in significant densification during sintering, hence complementing the flowability results as given in table 2. Further, findings are being manifested by the surface plots in figures 6(b-c). In this graphical representations, the effect of coal-fly ash wt % is pertinent indicating the maximum density found at minimum wt% of coal-fly ash and vice-versa as shown in figure 6(b) [47]. The combined effects of the sintering temperature and the compacting load on the density are exhibited in figure6(c). Though, the effect of the coal-fly ash wt % is more significant as compared to the sintering temperature and the compacting load. However, enhancement in sintered density with the increased temperature confirms the diffusion

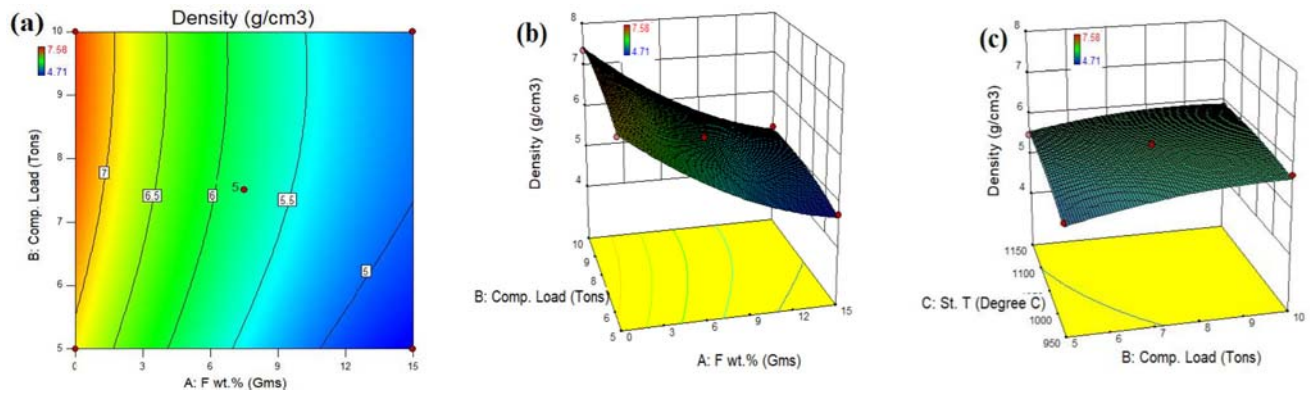

Figure 6. Plots for the sintered density: (**a**) contour for compacting load and coal-fly ash content, (**b**) surface plot for compacting load and coal-fly ash content, (**c**) surface plot for sintering temperature and compacting load.

Table 6. Modified ANOVA table for microhardness.

Source of variation	Sum of squares	Degree of freedom	Mean square	F value	P-value	
Regression	4038.69	9	448.74	14.44	0.0010	Significant
A (Coal-fly ash wt %)	2701.13	1	2701.13	86.91	< 0.0001	
B (Compacting load)	301.13	1	301.13	9.66	0.0171	
C (Sintering temperature)	480.50	1	480.50	15.46	0.0057	
Residual error	217.55	7	31.08			
Lack of fit	10.75	3	3.58	0.069	0.9734	not significant
Pure error	206.80	4	51.70			
Total	4256.24	16				
$R^2 = 0.94$, R^2(adj.) $= 0.88$						

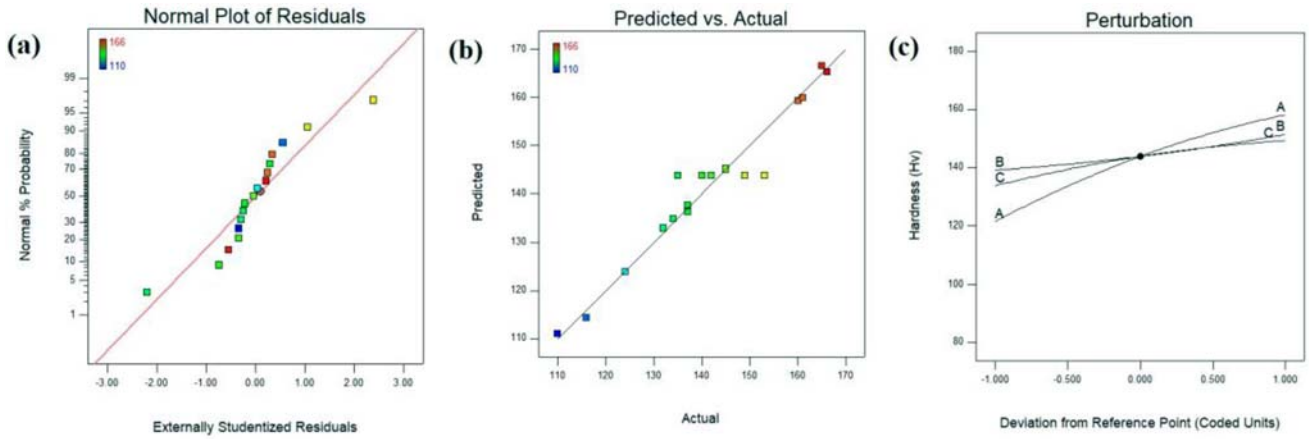

Figure 7. Plots for the microhardness: (**a**) normal probability, (**b**) predicted vs. actual and (**c**) perturbation.

of matrix particles. It can be deduced that the diffusion of the matrix particles reduced the porosity and coal-fly ash particles got mechanically locked. Hence, it can be inferred that the sintered density improves with the increased compacting load and the sintering temperature. On the other hand, the sintered density declines significantly with increasing coal-fly ash wt %. This is one of the prerequisite inherent properties of composites inculcating the higher specific mechanical properties [48].

3.8b *Statistical analysis of microhardness*: From the ANOVA table 6, it can be deduced that the coal-fly ash wt. % is the most prominent input parameter as it bears maximum F-value of 86.91. Since F-value of the model is 14.44, which renders the significance of the model. The values close to each other are complementing the significance of the model. The normal probability plot of residuals of microhardness is shown in figure 7(a). This is indicating the suitability of the data to be analysed further. The scattered data along the straight line in figure7(b) is showing enough scattered data around the straight line without following any specific trend. The scattering and location of the data in the vicinity of the straight line further advocating the usefulness of the data. The contribution of each input variable in affecting the microhardness of IMMCs is depicted in the form of a regression equation (8) as given below:

$$\mathrm{Hv} = 143.80 + 18.38 \times \mathrm{A} + 6.13 \times \mathrm{B} + 7.75 \times \mathrm{C} \quad (8)$$

In addition to the statistical significance of coal-fly ash reinforcement, the overall effect of the various input variables on the microhardness is depicted graphically in figures 8(a-d). With the increase in compaction loads, the microhardness increases at lower wt % of coal-fly ash whereas, at higher levels of coal-fly ash no significant effect is witnessed as shown in figure 8(b). Minimum microhardness is found at the minimum load and vice-versa.

The coal-fly ash wt % is found to be the dominant input variable affecting the microhardness of IMMCs i.e., on increasing the wt. % the microhardness increases almost linearly. The plot shown in figure 8(c) is showing a combined effect of sintering temperature and wt% of coal-fly ash on the microhardness. It can be observed that with an increase in the sintering temperature, the microhardness also increases. This is evident that sufficient diffusion among the matrix particles has taken place during solid-state sintering. Whereas, the effect of coal-fly ash wt% is similar as discussed for figure 8(b). A combined effect of the sintering temperature and the compacting load on the

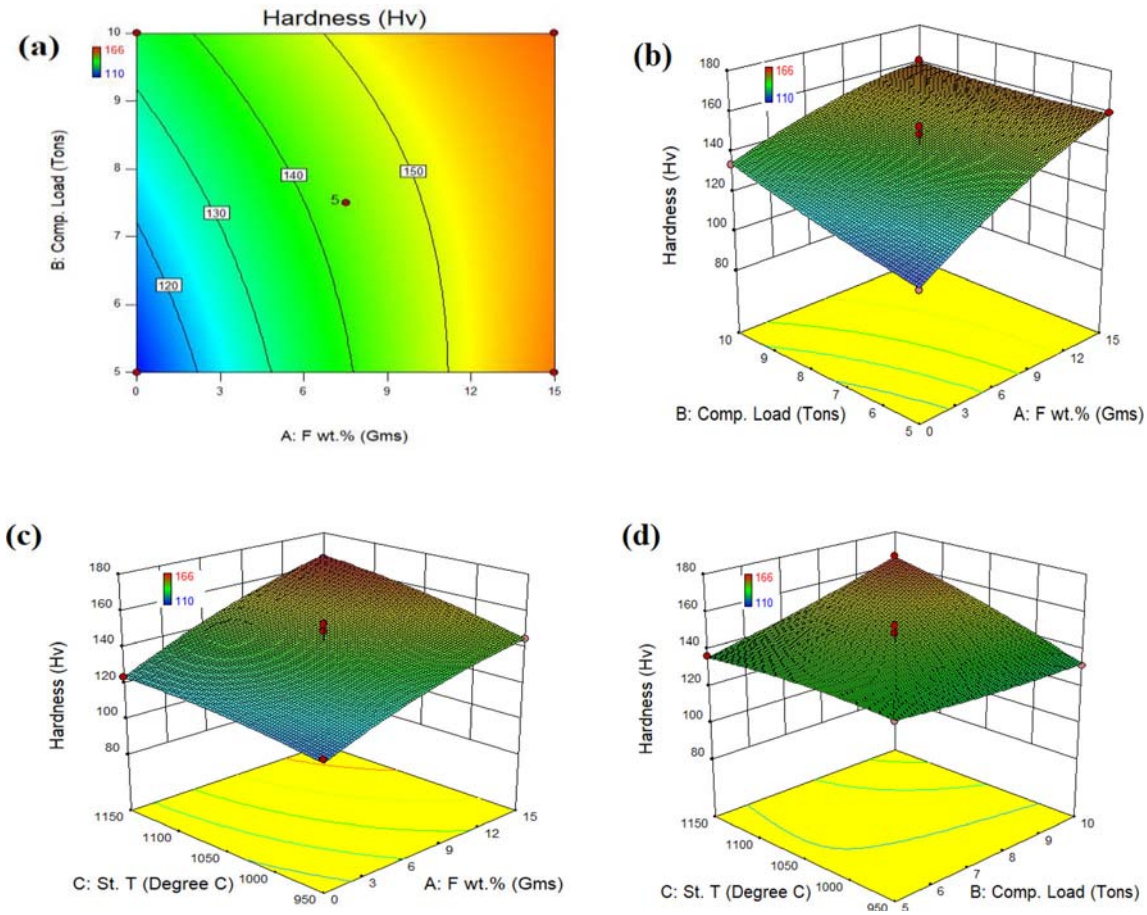

Figure 8. Exhibiting combined effects of input variables on hardness: (**a**) contour plot showing the effect of compacting load and coal-fly ash wt %, (**b**) surface plot showing the effect of compacting load and coal-fly ash wt %, (**c**) surface plot showing the effect of sintering temperature and coal-fly ash wt% and (d) surface plot showing the effect of sintering temperature and compacting load.

microhardness is another important concern which needs to be explained based on the surface plot as shown in figure 8(d). The maximum value of the microhardness is found at maximum sintering temperature and compacting load i.e., 1150°C and 10 tons, respectively [49].

4. Conclusions

The successful synthesization of iron metal-matrix composites (IMMCs) through powder metallurgy method has been demonstrated through uniform distribution, structural stability and interface bonding of the reinforcement with the matrix. The following specific conclusions have been drawn from the characterizations of IMMCs followed by their statistical analysis:

I. The FESEM analysis exhibited the uniform distribution of coal-fly ash particles in the iron matrix with clear interfaces. This entails the suitability of the reinforcement and the matrix combination for fabricating IMMCs using powder metallurgy techniques.
II. There was no evidence regarding the formation of new phases or compounds found in the XRD peaks, which implies that the sintering temperature ranges between 950°C and 1150°C.
III. There were no chemical reactions observed between the matrix and the reinforcement which indicates the optimal temperature range for IMMCs fabrication.
IV. The maximum 15 wt % coal-fly ash amplified the microhardness of IMMCs by 50 % and reduced the density by 35 % as compared to 0 wt % coal- fly ash.
V. Among the input variables, coal-fly ash wt.% found to be the most dominating input variable influencing the density and the microhardness of IMMCs.
VI. With an increase in wt % of reinforcement, the contribution of strengthening mechanisms responsible for enhanced microhardness changed from Hall–Petch effect at 0wt% to Load-transfer followed by

Hall–Petch effect and Taylor strengthening at 15 wt % of reinforcement.

VII. The experimentally observed microhardness of IMMCs was found significantly higher than that of the corresponding analytically calculated.

References

[1] Singh J and Chauhan A 2019 A review of microstructure, mechanical properties and wear behavior of hybrid aluminium matrix composites fabricated via stir casting route. *Sadhana* 44:1–18

[2] Ahmaruzzaman M 2010 A review on the utilization of fly ash. *Prog. Energy.and Combust. Sci*. 36:327–363

[3] Kim S H, and Hahn H T 2006 Size effect in particulate metal matrix composites: An analytical approach. *Adv. Compos. Mater*. 15:175–191

[4] Fulekar M H and Dave J M 1986 Disposal of fly ash — an environmental problem. *Int. J. Environ. Stud.* 26:191–215

[5] Manimaran R, Jayakumar I, Giyahudeen R M and Narayanan L 2018 Mechanical properties of fly ash composites — A review. *Energy Sources Part A*. 40:887–893

[6] Mishra D P and Das S K 2010 A study of physico-chemical and mineralogical properties of Talcher coal fly ash for stowing in underground coal mines. *Mater. Charact.* 61:1252–1259

[7] Guo R Q and Rohatgi P K 1997 Preparation of aluminium–fly ash particulate composite by powder metallurgy technique. *J. Mater. Sci*. 32:3971–3974

[8] Slipenyuk A, Kuprin V, Milman Y, Spowart J E and Miracle D B 2004 The effect of matrix to reinforcement particle size ratio (PSR) on the microstructure and mechanical properties of a P/M processed AlCuMn/SiCp MMC. *Mater. Sci. Eng. A*. 381:165–170

[9] Zhang B, Yang F, Qin Q, Lu T, Sun H and Lin S 2019 Characterisation of powder metallurgy H13 steels prepared from water atomised powders. *Powder Metall.* 2019:1–10

[10] Jha P, Gupta P, Kumar D and Parkash O 2014 Synthesis and characterization of Fe-ZrO_2 metal matrix composites. *J. Compos. Mater.* 48:2107–2115

[11] Meti V K V, Shirur S, Nampoothiri J, Ravi K R and Siddhalingeshwar I G 2018 Synthesis, Characterization and Mechanical Properties of AA7075 Based MMCs Reinforced with TiB_2 Particles Processed Through Ultrasound Assisted In-Situ Casting Technique. *Trans. Indian Inst. Met.* 71:841–848

[12] Sahoo S, Jha B B, Sahoo T K and Mandal A 2017 Influence of reinforcement and processing on steel-based composites: Microstructure and mechanical response. *Mater. Manuf. Process*. 33:564–571

[13] Abdollahi H, Mahdavinejad R and Leavoli R P 2015 Investigation and optimization of properties of sintered iron / recycled grey cast iron powder metallurgy parts. *J. Eng. Manuf*. 229:1010–1020

[14] Zhang X, Ma F, Ma K and Li X 2012 Effects of Graphite Content and Temperature on Microstructure and Mechanical Properties of Iron-Based Powder Metallurgy Parts. *J. Mater. Sci. Res*. 1:48–56

[15] Sharma Shyam, Hundekar P R, Gupta P, Kumar D, Jain R, Singh N and Rawat V 2017 Structural and mechanical characterization of re-pressed and annealed iron-alumina metal matrix nanocomposites. *J. Compos. Mater*. 52:1541–1556

[16] Gupta P, Kumar D, Parkash O and Jha A K 2014 Sintering and Hardness Behavior of Fe-Al_2O_3 Metal Matrix Nanocomposites Prepared by Powder Metallurgy. *J. Compos*. 2014:1–10

[17] Sahoo S, Jha B B, Mahata T and Sharma J 2019 Mechanical and Wear Behaviour of Hot-Pressed 304 stainless Steel Matrix Composites Containing TiB_2 Particles. *Trans. Indian Inst. Met*. 72:1153–1165

[18] Guo R Q, Rohatgi P K and Nath D 1996 Compacting characteristics of aluminium-fly ash powder mixtures. *J. Mater. Sci*. 31:5513–5519

[19] Rajan S T K, Balaji A N, Narayanasamy P and Vettivel S C 2018 Microstructural, electrical, thermal and tribological studies of copper-fly ash composites through powder metallurgy. *Bull POLISH Acad. Sci*. 66:935–940

[20] Saker A, Cares-Pacheco M G, Marchal P and Falk V 2019 Powders flowability assessment in granular compaction: What about the consistency of Hausner ratio? *Powder Technol*. 354:52–63

[21] Verma P, Saha R and Chaira D 2018 Waste steel scrap to nanostructured powder and superior compact through powder metallurgy: Powder generation, processing and characterization. *Powder Technol*. 326:159–167

[22] Gao X, Zhang X, Qian M and Geng L 2019 Effect of reinforcement shape on fracture behaviour of SiC/Al composites with network architecture. *Compos. Struct.* 215:411–420

[23] Singh J, Verma V, Kumar R, and Kumar R 2019 Influence of Mg^{2+}-substitution on the optical band gap energy of $Cr_{2-x}Mg_xO_3$ nanoparticles. *Results Phys.* 13:1–8

[24] Prasad D S, Shoba C and Ramanaiah N 2014 Investigations on mechanical properties of aluminum hybrid composites. *J. Mater. Res. Technol.* 3:79–85

[25] Matsunaga T, Kim J K, Hardcastle S and Rohatgi P K 2002 Crystallinity and selected properties of fly ash particles. *Mater. Sci. Eng.* 325:333–343

[26] Raj R and Thakur D G 2019 Effect of particle size and volume fraction on the strengthening mechanisms of boron carbide reinforced aluminum metal matrix composites. *J. Mech. Eng. Sci*. 233:1345–1356

[27] Kim C S, Sohn I, Nezafati M, Ferguson J B, Schultz B F, Bajestani-Gohari Z, Rohatgi P K and Cho K 2013 Prediction models for the yield strength of particle-reinforced unimodal pure magnesium (Mg) metal matrix nanocomposites (MMNCs). *J. Mater. Sci.* 48:4191–4204

[28] Chidambaram A, Balasivanandha Prabu S and Padmanabhan KA 2019 Microstructure and mechanical properties of AA6061–5wt. %TiB_2 in-situ metal matrix composite subjected to equal channel angular pressing. *Mater. Sci. Eng.* 759:762–769

[29] Zhao L, Lu H and Gao Z 2015 Microstructure and Mechanical Properties of Al/Graphene Composite Produced by High-Pressure Torsion. *Adv. Eng. Mater*. 17: 976–981

[30] Balakrishna Bhat T and Arunachalam VS 1980 Strengthening mechanisms in alloys. *Indian Acad.Sci*. 3:275–296

[31] Sanaty-Zadeh A 2012 Comparison between current models for the strength of particulate-reinforced metal matrix nanocomposites with emphasis on consideration of Hall–Petch effect. *Mater. Sci. Eng. A*. 531:112–118

[32] Sahoo S K, Sahoo B N and Panigrahi S K 2020 Effect of in-situ sub-micron sized TiB_2 reinforcement on microstructure and mechanical properties in ZE41 magnesium matrix composites. *Mater. Sci. Eng*. 773:1–39

[33] Azadi M, Rezanezhad S, Zolfaghari M and Azadi M 2020 Investigation of tribological and compressive behaviors of Al/SiO2 nanocomposites after T6 heat treatment. *Sadhana* 45:1–13

[34] Xi L, Gu D, Guo S and Wang R 2020 Grain refinement in laser manufactured Al-based composites with TiB_2 ceramic. *J. Mater. Res. Technol.* 9:2611–2622

[35] Ramakrishnan N 1996 An analytical study on strengthening of particulate reinforced metal matrix composites. *Acta Mater*. 44:69–77

[36] Chelliah N M, Singh H and Surappa M K 2017 Microstructural evolution and strengthening behavior in in-situ magnesium matrix composites fabricated by solidification processing. *Mater. Chem. Phys*. 194:65–76

[37] Rohatgi P K, Gupta N and Alaraj S 2006 Thermal expansion of aluminum-fly ash cenosphere composites synthesized by pressure infiltration echnique. *J. Compos. Mater*. 40:1163–1174

[38] Zhou X L, Dong Y H, Hua X Z and Ye Z G 2010 Effect of Fe on the sintering and thermal properties of Mo-Cu composites. *Mater. Des*. 31:1603–1606

[39] Yazdi A Z, Bagheri R, Zebarjad S M and Hesabi Z R 2010 Incorporating aspect ratio in a new modeling approach for strengthening of MMCs and its extension from micro to nano scale. *Adv. Compos. Mater*. 19:299–316

[40] Balasubramanian M 2013 *Dispersed Phase Composite materials and processing*. BoCa Raton, London, New York: CRC Press Taylor & Francis Group. 77

[41] David Raja Selvam J, Robinson Smart D S and Dinaharan I 2013 Microstructure and some mechanical properties of fly ash particulate reinforced AA6061 aluminum alloy composites prepared by compocasting. *Mater. Des*. 49:28–34

[42] Saba F, Zhang F, Liu S and Liu T 2019 Reinforcement size dependence of mechanical properties and strengthening mechanisms in diamond reinforced titanium metal matrix composites. *Compos. Part B* .167:7–19

[43] Bahador A, Umeda J, Hamzah E, Yusof F, Li X and Kondoh K 2020 Synergistic strengthening mechanisms of copper matrix composites with TiO_2 nanoparticles. *Mater. Sci. Eng. A*. 772:1387–1397

[44] Yang H, Jiang L, Balog M, Krizik P and Schoenung J M 2017 Reinforcement Size Dependence of Load Bearing Capacity in Ultrafine-Grained Metal Matrix Composites. *Metall. Mater. Trans. A*. 48:4385–4892

[45] Ferguson J B, Schultz B F, Venugopalan D, Lopez H F, Rohatgi P K, Cho K and Kim S 2014 On the superposition of strengthening mechanisms in dispersion strengthened alloys and metal-matrix nanocomposites: Considerations of stress and energy. *Met. Mater. Int*. 20:375–388

[46] Balamurugan P and Uthayakumar M 2015 Influence of process parameters on Cu-fly ash composite by powder metallurgy technique. *Mater. Manuf. Process.* 30:313–319

[47] Siddhi Jailani H, Rajadurai A, Mohan B, Senthil Kumar A and Sornakumar T 2011 Development and properties of aluminium silicon alloy fly ash composites. *Powder Metall.* 54:474–479

[48] Prajapati P K and Chaira D 2019 Fabrication and Characterization of Cu–B 4 C Metal Matrix Composite by Powder Metallurgy: Effect of B_4C on Microstructure, Mechanical Properties and Electrical Conductivity. Trans. *Indian Inst. Met.* 72:673–684

[49] Tiwari S, Rajput P and Srivastava S 2012 Densification Behaviour in the Fabrication of Al-Fe Metal Matrix Composite Using Powder Metallurgy Route. *ISRN Metall*. :1–8